MIT Open Access Articles

SEARCHING FOR THE 3.5 keV LINE IN THE STACKED SUZAKU OBSERVATIONS OF GALAXY CLUSTERS

Massachusetts Institute of Technology

SEARCHING FOR THE 3.5 keV LINE IN THE STACKED *SUZAKU* OBSERVATIONS OF GALAXY CLUSTERS

ESRA BULBUL[1], MAXIM MARKEVITCH[2], ADAM FOSTER[3], ERIC MILLER[1], MARK BAUTZ[1],
MIKE LOEWENSTEIN[2], SCOTT W. RANDALL[3], AND RANDALL K. SMITH[3]

[1] Kavli Institute for Astrophysics & Space Research, Massachusetts Institute of Technology,
77 Massachusetts Avenue, Cambridge, MA 02139, USA; ebulbul@mit.edu
[2] NASA Goddard Space Flight Center, Greenbelt, MD, USA
[3] Harvard-Smithsonian Center for Astrophysics, 60 Garden Street, Cambridge, MA 02138, USA

ABSTRACT

We perform a detailed study of the stacked *Suzaku* observations of 47 galaxy clusters, spanning a redshift range of 0.01–0.45, to search for the unidentified 3.5 keV line. This sample provides an independent test for the previously detected line. We detect a 2σ-significant spectral feature at 3.5 keV in the spectrum of the full sample. When the sample is divided into two subsamples (cool-core and non-cool core clusters), the cool-core subsample shows no statistically significant positive residuals at the line energy. A very weak ($\sim 2\sigma$ confidence) spectral feature at 3.5 keV is permitted by the data from the non-cool-core clusters sample. The upper limit on a neutrino decay mixing angle of $\sin^2(2\theta) = 6.1 \times 10^{-11}$ from the full *Suzaku* sample is consistent with the previous detections in the stacked *XMM-Newton* sample of galaxy clusters (which had a higher statistical sensitivity to faint lines), M31, and Galactic center, at a 90% confidence level. However, the constraint from the present sample, which does not include the Perseus cluster, is in tension with previously reported line flux observed in the core of the Perseus cluster with *XMM-Newton* and *Suzaku*.

Key words: dark matter – galaxies: clusters: general – large-scale structure of universe – line: identification

1. INTRODUCTION

The detection of an unidentified emission line near 3.5 keV in the stacked *XMM-Newton* observations of galaxy clusters, and in the Perseus cluster, has received significant attention from astrophysics and particle physics communities (Bulbul et al. 2014a, Bu14a hereafter). The detection was also reported in the outskirts of the Perseus cluster and the Andromeda galaxy observed with *XMM-Newton* (Boyarsky et al. 2014, Bo14 hereafter), as well as in *Suzaku* observations of the Perseus cluster core (Urban et al. 2015; Franse et al. 2016; see, however, a non-detection by Tamura et al. 2015). An emission line at a consistent energy was detected in the *XMM-Newton* and *Chandra* observations of the Galactic center, and in eight other individual clusters (Boyarsky et al. 2015; Iakubovskyi et al. 2015; Jeltema & Profumo 2015).

Although the line was detected by several X-ray detectors in a variety of objects, the origin of the line is unclear. Bu14a discussed potential astrophysical origins of this line, e.g., an emission line from the nearby weak atomic transitions of K XVIII and Ar XVII dielectronic recombination (DR); they found that these lines have to be 10–20 times above the model prediction. Jeltema & Profumo (2015) and Carlson et al. (2015) suggested that a large fraction of cool gas with $T < 1$ keV in cluster cores may produce lines from K XVIII stronger then those Bu14a allowed for. We commented in Bulbul et al. (2014b; hereafter, Bu14b) that ratios of the observed lines from other elements exclude significant quantities of such cool gas. Recently, Gu et al. (2015) suggested that charge exchange between sulfur ions and neutral gas, a process not included in Bu14a, may produce excess near 3.5 keV. These, as well as some other recent spatially resolved studies, are reviewed by Franse et al. (2016).

A more exotic possibility that is interesting to consider is that the observed line is a signal from decaying dark matter particles (Abazajian 2014; Horiuchi et al. 2016). In previous studies, they reported that the flux of the line is consistent across objects of different mass (Andromeda galaxy, stacked galaxy clusters, and Galactic center) when the mass scaling in decaying dark matter models are taken into account (see Boyarsky et al. 2015). Although it is challenging to test this hypothesis with the current CCD (100–120 eV) resolution X-ray telescopes, the radial distribution of the line in a well-exposed galaxy cluster may provide further information on its origin. Franse et al. (2016) examined the flux distribution of the 3.5 keV line, as a function of radius in the Perseus cluster. However, the observed line flux from the Perseus core ($r \leqslant 1'$) appears to be in tension with detection from other objects, assuming the decaying dark matter model (Bu14a, Franse et al. 2016). Franse et al. (2016) found that the profile of the line is consistent with a dark matter origin, as well as with an unknown astrophysical line. Recently, Ruchayskiy et al. (2015) have analyzed a very deep *XMM-Newton* observation of the Draco dwarf galaxy. They found no line signal in the spectrum from the MOS detectors and a 2.3σ-significant hint of a positive signal at the right energy in the independent PN spectrum, both findings consistent with the previous detections within uncertainties.

Bu14a laid the framework for stacking X-ray observations at the rest frame and successfully applied this method to a large sample of *XMM-Newton* observations. In this work, we take a step further to search for the unidentified line in the stacked *Suzaku* observations of 47 galaxy clusters. This paper is organized as follows. Section 2 describes the data processing and spectra stacking. In Sections 3 and 4, we provide our results and conclusions. All errors quoted throughout the paper correspond to 68%(90%) single-parameter confidence intervals; upper limits are at 90% confidence, unless otherwise stated. Throughout our analysis, we used a standard ΛCDM

cosmology with $H_0 = 71 \, \mathrm{km \, s^{-1} \, Mpc^{-1}}$, $\Omega_M = 0.27$, and $\Omega_\Lambda = 0.73$. In this cosmology, $1'$ corresponds to ~ 0.11 Mpc at redshift of 0.1.

2. SAMPLE SELECTION AND DATA REDUCTION

In an attempt to smooth the instrumental and background features related to the *Suzaku* XIS detectors, we select a sample of galaxy clusters based on the number of X-ray counts in their 2–10 keV band. To be able to smear the instrumental features, by blue-shifting the spectra to the source frame, we select clusters covering a large redshift range of $0.01 < z < 0.45$. A significant number of on-axis X-ray observations of galaxy clusters have been performed by *Suzaku* since its launch in 2005. We selected observations with a minimum of 10,000 counts in $z < 0.2$ per cluster, and 5000 counts per cluster for clusters with redshifts $0.2 < z < 0.44$. The final sample includes 51 *Suzaku* X-ray observations of 47 galaxy clusters. The details of the observations are summarized in Table 1, along with the filtered exposure times. The filtering process is described below. We note that the Perseus cluster, which is the brightest cluster in terms of X-rays, has the longest observations (1Ms) available in the *Suzaku* archive. However, to avoid the final stacked spectrum being dominated by this cluster, we exclude it from our sample. The flux distribution of the 3.5 keV line out to the virial radius of the Perseus cluster has already been studied in great detail by Franse et al. (2016).

The details of *Suzaku* data reduction are described in Bulbul et al. (2016) and Franse et al. (2016). Here, we provide a summary of the steps we follow in the data analysis. After the calibrated data is filtered from the background flares, source images in the 0.4–7.0 keV band are extracted from the filtered event files. These images are used to detect point sources within the *Suzaku* the field-of-view (FOV) using the CIAO's tool *wavdetect*. The detected point sources are excluded from the further analysis.

The source and particle background spectra are extracted from the filtered event file and filtered night-time Earth data using the FTOOL *xisnxbgen*. The spectra are extracted within the overdensity radius R_{500},[4] if the estimated R_{500} falls within FOV of XIS.

The overdensity radii (R_{500}) are calculated using the mass-temperature scaling relation for each cluster (Vikhlinin et al. 2009). The temperatures used in these estimates are obtained from previously published results in the literature. For some of the nearby clusters, R_{500} is larger than the XIS FOV. For those, we use the largest possible region (a circle with a radius of $8'.3$) that encompasses the cluster center while avoiding the detector edges. The extraction radii for the full sample are given in Table 3. Redistribution matrix files (RMFs) and ancillary response files (ARFs) are constructed using the FTOOLs *xisarfgen* and *xisrmfgen*.

The particle-induced background spectrum is subtracted from each source spectrum, prior to fitting. Following the same approach presented in Bu14a, we first perform the spectral fitting in the Fe Kα band (5.5–7.5 keV rest frame) with a single temperature thermal model (*apec*) to determine the best-fit redshift of each cluster with the AtomDB version 2.0.2 (Smith

---

[4] The overdensity radius R_{500} is defined as the radius within which the average matter density of the cluster is 500 times the critical density of the universe at the cluster redshift.

et al. 2001; Foster et al. 2012). XSPEC v12.9.0 is used to perform the spectral fits (Arnaud 1996) with the extended χ^2 statistics as an estimator of the goodness-of-fits. The spectral counts in each energy bin were sufficiently high to allow the use of the Gaussian statistics in this analysis (Protassov et al. 2002).

We combine front-illuminated (FI) XIS0 and XIS3 data to increase the signal-to-noise, whereas the back illuminated (BI) XIS1 data are modeled independently, due to the difference in energy responses. The best-fit redshifts (z_{best}) obtained from FI observations are given in Table 1. The best-fit redshifts measured from BI observations are in good agreement with FI observations.

In order to detect a weak spectral feature, such as the ~ 3.5 keV line ($\sim 1\%$ excess over the continuum), the detector and background artifacts must be eliminated from the high signal-to-noise stacked galaxy cluster spectrum. In order to accomplish this, we stacked the spectra of our selected 47 clusters at the source frame using the best-fit X-ray redshift of each observation determined above. The energies of the source and background X-ray events are rescaled to the source frame using the best-fit redshifts. The spectra within R_{500} are extracted from these rescaled event and background files, before being stacked. The individual RMFs and ARFs are then remapped to the source frame. The weighting factors (ω_{cnts}), given in Table 3, for stacking RMFs and ARFs are calculated using the total counts in the fitting band (2–10 keV). The weighted and remapped ARFs and RMFs are combined using the FTOOLs *addarf* and *addrmf*, while *mathpha* is used to produce stacked source and background spectra. At the end of the stacking processes, we obtain a total of 5.4 Ms FI and 2.7 Ms BI galaxy cluster observations in the full sample. These count-weighted response files are used in modeling the continuum and the known plasma emission lines (see Section 3).

3. RESULTS

As in B14a, We fit the background-subtracted stacked source spectra with line-free multi-temperature *apec* models to represent the continuum emission with high accuracy. Gaussian models are added to account for individual atomic lines in the 1.95–6 keV energy band. Our total model includes the following lines at their rest energies: Al XIII (2.05 keV), Si XIV (2.01, 2.37, and 2.51 keV), Si XII (2.18, 2.29, and 2.34 keV), S XV (2.46, 2.88, 3.03 keV), S XVI (2.62 keV), Ar XVII (triplet at 3.12, 3.62, 3.68 keV), Cl XVI (2.79 keV), Cl XVII (2.96 keV), Cl XVII (3.51 keV), K XVIII (triplet 3.47, 3.49 and 3.51 keV), K XIX (3.71 keV), Ca XIX (complex at 3.86, 3.90, 4.58 keV), Ar XVIII (3.31, 3.93 keV), Ca XX (4.10 keV), and Cr XXIII (5.69 keV).

After the first fit iteration, the χ^2 improvement for the inclusion of each of these lines is determined, and the lines that are detected with $< 2\sigma$ are removed from the model. Additionally, a power-law model, with an index of 1.41 and free normalization, is added to the total model to account for the contribution of the cosmic X-ray background (CXB). We note that Galactic halo emission is negligible in this energy band; hence, it is not included in the model. The best-fit temperatures, normalizations of the *line-free apec* models, and the fluxes of S XV, S XVI, Ca XIX, and Ca XX lines are given in Table 2.

Table 1
On-axis Galaxy Cluster Observations Performed by *Suzaku*

Cluster	R.A.	Decl.	ObsID	FI Exp (ks)	BI Exp (ks)	z_{best}	Sub-sample
Fornax	3 38 33.48	−35.0 29 30.5	100020010	137.5	68.7	0.004	CC
Antlia	10 30 2.21	−35.0 19 39.7	802035010	112.5	56.2	0.012	NCC
Centaurus	12 48 48.29	−41 18 47.5	800014010	61.4	30.7	0.008	CC
A1060	10 36 41.86	−27.0 31 51.6	800003010	64.9	32.4	0.012	CC
A3627	16 14 16.13	−60.0 50 59.6	803032010	87.7	43.8	0.017	NCC
AWM7	02 5 29.5	41 34 18	801035010	32.1	16.0	0.014	CC
A262	1 52 46.13	36.0 9 32.8	802001010	67.6	33.8	0.017	CC
A3581	14 07 37.99	−27.0 01 11.6	807026010	129.4	64.7	0.022	CC
Coma	12 57 33.43	26.0 55 34.0	801097010	326.3	163.1	0.021	NCC
Ophiuchus	17 12 26.23	−23.0 22 44.4	802046010	162.8	81.4	0.029	CC
A2199	16 28 46.13	39.0 29 2.4	801056010	35.5	18.0	0.031	CC
A496	04 33 38.4	−13 15 33 .0	803073010	68.68	34.4	0.032	CC
A3571	13 47 26.98	−32.0 51 8.6	808094010	69.8	34.9	0.038	NCC
Triangulum Australis	16 38 29.4	−64.0 20 51.7	803028010	138.8	69.4	0.048	NCC
A754	09 08 50.71	−9.0 38 10.0	802063010	182.8	91.4	0.054	NCC
A2665	23 50 51.86	6.0 08 6.7	801076010	23.1	11.5	0.099	NCC
A3667	20 12 33.84	−56.0 47 50.6	801096010	40.4	20.2	0.055	NCC
AS1101	23 13 59.02	−42.0 43 53.0	801093010	107.0	53.55	0.055	CC
A2256	17 4 3.31	78.0 42 40.3	801061010	188.7	94.3	0.055	NCC
A1831	13 59 12.17	27.0 58 9.5	801077010	32.7	16.3	0.078	NCC
A1795	13 48 53.78	26.0 36 3.6	800012010	19.6	9.8	0.063	CC
A3112	03 17 59.57	−44.0 15 2.5	808068020	109.9	54.9	0.075	CC
			803054010	226.9	113.5		
			808068010	108.8	54.4		
A1800	13 49 26.83	28 05 50.3	801078010	35.6	17.8	0.075	NCC
A2029	15 10 57.82	05 44 59.3	804024010	13.9	6.9	0.076	CC
A2495	22 50 15.89	10 55 18.5	801080020	49.9	24.9	0.078	⋯
A2061	15 21 14.28	30 38 43.1	801081010	21.7	10.8	0.081	CC
A2249	17 9 50.4	34 29 6.4	801082010	45.6	22.8	0.085	⋯
A1750	13 30 49.9	−01 52 22	806095010	76.0	38.0	0.089	CC
A272	01 55 2.47	33 54 9.4	801084010	41.9	20.9	0.093	⋯
A2218	16 36 1.25	66 12 18.0	100030010	60.0	30.0	0.173	NCC
			800019010	81.1	40.5		
MS2216.0-0401	22 18 39.1	−03 46 9.5	807085010	49.7	24.8	0.094	⋯
A2142	15 58 7.49	27 17 16.4	801055010	95.0	47.5	0.091	NCC
A2244	17 2 45.24	34 3 0.7	802078010	130.9	65.4	0.098	CC
A566	07 4 21.96	63 15 52.9	801085010	43.5	21.7	0.096	⋯
PKS0745-191	07 47 32.45	−19 17 24.4	802062010	55.4	27.7	0.103	CC
A1674	13 03 52.22	67 32 49.6	801062010	126.3	63.1	0.151	NCC
A2811	00 41 52.87	−28 33 18.7	800005010	53.3	26.6	0.107	NCC
A115	00 55 58.54	26 22 48.7	805077010	123.8	61.9	0.195	CC
A1246	11 23 50.0	21 25 31	804028010	88.0	44.0	0.193	NCC
A2219	16 40 17.02	46.0 43 12.0	804011010	170.	85.0	0.225	NCC
A2390	21 53 35.5	17 41 12.0	804012010	174.0	87.0	0.228	CC
ZWCL2341.1+0000	23 43 38.81	00 19 49.1	803001010	82.2	41.1	0.273	NCC
A2537	23 8 21.48	−2 11 10	805090010	201.3	100.6	0.291	CC
Bullet	06 58 48.96	−55 55 58.8	801089010	164.8	82.4	0.297	NCC
A2744	00 14 9.53	−30 20 40.6	802033010	250.2	125.1	0.304	CC
MS1512.4+3647	15 14 25.42	36 37 11.3	802034010	466.2	233.1	0.367	CC
RXCJ1347.5-1145	13 47 30.6	−11 45 10	801013010	114.3	57.1	0.451	CC
	13 47 25.39	−01 10 48 34.2	801013020	138.3	69.1	0.450	

Note. Columns are coordinates (R.A., decl.), *Suzaku* observation ID, exposure in front-illuminated (XIS0+XIS3) and back-illuminated (XIS1) observations, best-fit redshifts obtained from fits of Fe–K band of FI observations, and the category and subsample of the cluster as determined based on the state of the core. NCC stands for non-cool core sample, while CC stands for cool-core sample.

It is crucial to accurately determine the fluxes of the nearby atomic lines of K XVIII, Cl XVII, and Ar XVII in order to be able to measure the flux of the unidentified line at 3.5 keV. The line ratios of S XV at 2.46 keV to S XVI at 2.62 keV and Ca XIX at 3.9 keV to Ca XX at 4.1 keV are good diagnostics tools for estimating plasma temperature, especially valuable for detecting the presence of cool gas (Bu14b). Following the same

method presented in Bu14a, we determine the plasma temperature based on the measured fluxes of helium-like S XV at 2.46 keV, hydrogen-like S XVI at 2.63 keV, and helium-like Ca XIX and hydrogen-like Ca XX lines at 3.90 keV and 4.11 keV from the spectral fits. However, the band where S XV and S XVI are located is crowded with strong Si XIV lines. Therefore, we tie the fluxes of Si XIV

Table 2
Measured and Estimated Model Parameters

Parameters	Full Sample		Cool Core Clusters		Non Cool-core Clusters	
	FI	BI	FI	BI	FI	BI
Measured Values:						
kT_1 (keV)	5.9 ± 0.3	4.8 ± 0.4	6.8 ± 0.4	3.0 ± 0.6	3.1 ± 0.3	2.9 ± 0.2
N_1 (10^{-2} cm^{-5})	1.2 ± 0.2	1.9 ± 0.3	1.5 ± 0.6	1.4 ± 0.7	1.3 ± 0.2	1.6 ± 0.3
kT_2 (keV)	8.3 ± 0.3	9.56 ± 0.6	8.3 ± 0.6	9.7 ± 1.5	15.1 ± 1.23	17.1 ± 3.5
N_2 (10^{-2} cm^{-5})	1.0 ± 0.2	2.5 ± 0.4	1.5 ± 0.2	2.9 ± 0.4	2.9 ± 0.7	2.2 ± 0.9
kT_3 (keV)	9.9 ± 0.4	...	...	...	...	...
N_3 (10^{-2} cm^{-5})	1.2 ± 0.2	...	...	...	...	...
S XV (10^{-6} phts cm^{-2} s^{-1})	9.9 ± 1.2	7.8 ± 2.0	16.7 ± 1.4	11.7 ± 4.3	$1.4^{+2.2}_{-1.4}$	$3.2^{+4.7}_{-3.1}$
S XVI (10^{-6} phts cm^{-2} s^{-1})	26.6 ± 1.1	24.2 ± 1.8	32.1 ± 1.3	28.7 ± 1.9	15.6 ± 2.5	16.7 ± 3.2
Ar XVII (10^{-6} phts cm^{-2} s^{-1})	9.5 ± 1.1	7.9 ± 1.5	13.2 ± 1.3	9.1 ± 1.6	5.3 ± 2.0	6.6 ± 2.8
Ca XIX (10^{-6} phts cm^{-2} s^{-1})	4.6 ± 2.4	4.6 ± 2.0	7.1 ± 2.8	$6.1^{+3.1}_{-4.1}$	4.8 ± 1.4	4.9 ± 2.4
Ca XX (10^{-6} phts cm^{-2} s^{-1})	5.0 ± 0.7	6.07 ± 1.1	5.5 ± 0.9	5.5 ± 1.2	3.3 ± 1.2	3.5 ± 2.1
Estimated Values:						
kT (keV)	3.0	3.3	2.6	2.9	3.8[a]	3.8[a]
K XVIII (10^{-6} phts cm^{-2} s^{-1})	0.17	0.14	0.21	0.19	0.12	0.12
Cl XVII (10^{-6} phts cm^{-2} s^{-1})	0.08	0.08	0.09	0.09	0.08	0.08
Ar XVII DR (10^{-6} phts cm^{-2} s^{-1})	0.03	0.02	0.05	0.03	0.01	0.01

Note. Best-fit Temperature and normalizations of *line-free apec* Model in 1.95–6 keV fit to the stacked XIS FI/BI spectra for various samples. The line fluxes of the S XV, S XVI, Ar XVII, Ca XIX, and Ca XX are at rest energies 2.51, 2.63, 3.12, 3.90, and 4.11 keV. Ninety percent uncertainties are given. Lower panel shows the estimated maximum fluxes of the atomic lines in 3–4 keV band (before they are multiplied by a factor of 3) including K XVIII at 3.51 keV, Cl XVII at 3.521 keV, and Ar XVII DR line at 3.62 keV. The implied plasma temperatures are calculated based on S line ratios.
[a] The temperatures and line fluxes for NCC sample are determined from the Ca line ratio.

(2.01:2.37:2.51 keV) to each other with flux ratios of (21:3.5:1). The Si XIV line ratios are estimated based on the AtomDB predictions for 3–5 keV plasma. The measured fluxes are given in the top panel of Table 2.

The maximum fluxes of the K XVIII triplet (3.47:3.49:3.51 keV) with the ratios of (1:0.5:2.3) are then estimated using AtomDB, as described in Bu14a. Cl XVII Lyβ is also included in the fits, and the flux is tied to $0.15\times$ that of the Lyα line at 2.96 keV. We note that the Cl XVII Lyα line is not detected significantly in any of our samples; therefore, the Cl XVII Lyβ line is removed from our model after the first fit iteration. The maximum flux of the Ar XVII DR line flux at 3.62 keV is determined from the measured flux of Ar XVII triplet line at 3.12 keV. The expected flux of the Ar XVII DR line is <1% of the Ar XVII triplet at 3.12 keV for 3–5 keV plasma. The estimated fluxes of nearby lines (K XVIII at 3.51 keV, Cl XVII at 3.50 keV, and Ar XVII DR at 3.62 keV), as well as plasma temperatures based on S and Ca line ratios are given in Table 2, bottom panel. As in Bu14a, the lower and upper limits of the fluxes of K XVIII complex, Cl XVII, and Ar XVII DR lines are set to 0.1–3 times of the maximum predicted fluxes (estimates shown in Table 2 are before the multiplication) to account for abundance variance between different ions.

3.1. Full Sample

A total of 5.06×10^6 source counts in the 5.4 Ms FI observations and 2.9×10^6 source counts in the 2.7 Ms BI observations of the full sample are obtained in the 1.95–6 keV energy band. The count-weighted redshift of this sample is $z \sim 0.12$. After the first fit iteration with *line-free apec* and Gaussian models, we obtain a good fit to the stacked FI observations with χ^2 of 1032.3 for 1069 dof. The best-fit parameters of the model are given in Table 2. The predicted

plasma temperature indicated by the S XV to S XV line ratio is kT ~3.1 keV for this sample.

To explore the 3–4 keV band in the full sample (although the fit is performed in a wider 2–6 keV band), we add an Gaussian with a fixed energy at 3.54 keV (the best-fit energy of the line detected in the *Suzaku* observations of the Perseus cluster). The line width is fixed to zero because we do not expect that the line width is resolved with CCD-type detectors, regardless of its origin. The *Suzaku* FI and BI detectors have energy resolutions of 110–120 eV (similar energy resolution to EPIC detectors on *XMM-Newton*).

Here, we explore the possible interpretation of the 3.54 keV line as a decay feature of dark matter particles; therefore, we use the properly weighted response files to reflect the physical properties of each cluster and the stacked sample. We note that the proper X-ray counts-weighted response files are used to model the continuum and known atomic transitions, as described in Section 2.

The contribution of each cluster to any flux due to dark matter decay in the stacked sample is related to the mass of decaying dark matter particles within the FOV. Following the same formulation laid out by Bu14a, the weight of each cluster in the full *Suzaku* sample is;

$$\omega_{i,\mathrm{dm}} = \frac{M_{i,\mathrm{DM}}^{\mathrm{proj}}(<R_{\mathrm{ext}})(1 + z_i)}{4\pi D_{i,L}^2} \frac{e_i}{e_{\mathrm{tot}}}, \qquad (1)$$

where z_i is the redshift of the ith cluster, e_i and e_{tot} are the exposure time of the ith cluster and the total exposure time of the sample, $M_{\mathrm{DM}}^{\mathrm{FOV}}$ is the projected dark matter mass within the spectral extraction region (R_{ext}, which is either R_{500} or R_{FOV}), and D_L is the luminosity distance. We use the the Navarro–Frenk–White profile (Navarro et al. 1997) to determine the dark matter mass within the FOV. The steps in these calculation are described in detail in B14a. The calculated weight of each

Table 3
Properties of Each Cluster in the *Suzaku* Sample

Cluster	(1) R_{ext} (Mpc)	(2) M_{DM}^{proj} ($10^{14}M_\odot$)	(3) M_{DM}^{proj}/D_L^2 ($10^{10}M_\odot$ Mpc^{-2})	(4) ω_{cnt} (10^{-2})	(5) ω_{DM} (10^{-2})	Cluster	(6) R_{ext} (Mpc)	(7) M_{DM}^{proj} ($10^{14}M_\odot$)	(8) M_{DM}^{proj}/D_L^2 ($10^{10}M_\odot$ Mpc^{-2})	(9) ω_{cnt} (10^{-2})	(10) ω_{DM} (10^{-2})
Fornax	0.04	0.04	1.18	1.34	4.97	A2029	0.71	7.17	0.62	0.40	0.09
Antlia	0.10	0.18	0.98	0.61	3.41	A2495	0.69	2.63	0.24	0.29	1.02
Centaurus	0.12	0.41	1.55	3.18	2.93	A2061	0.72	3.89	0.33	0.15	0.17
A1060	0.13	0.39	1.19	1.66	2.38	A2249	0.74	5.64	0.45	0.28	0.49
A3627	0.16	1.03	2.33	1.87	6.34	A1750	0.78	2.34	0.16	0.29	1.12
AWM7	0.16	0.57	1.20	1.27	1.19	A272	0.78	2.58	0.18	0.20	0.22
A262	0.16	0.37	0.79	1.04	1.65	MS2216.0-0401	0.80	2.35	0.15	0.23	0.29
A3581	0.23	0.48	0.49	1.33	1.96	A2142	0.82	9.11	0.57	2.85	0.48
Coma	0.23	1.81	1.81	17.71	18.42	A2244	0.86	5.65	0.31	1.64	2.48
Ophiuchus	0.27	2.76	1.99	20.39	10.18	A566	0.87	3.32	0.18	0.16	0.45
A2199	0.29	2.03	1.26	1.32	1.40	PKS0745-191	0.91	7.76	0.37	1.57	0.33
A496	0.31	1.34	0.71	2.22	1.52	A1674	0.91	3.14	0.14	0.18	1.63
A3571	0.38	2.79	0.98	3.19	1.56	A2811	0.94	4.83	0.21	0.21	0.25
Triangulum	0.48	5.38	1.12	5.98	4.33	A2218	1.20	7.63	0.11	0.46	1.07
Australis	⋯	⋯	⋯	⋯	⋯	A1246	1.15	6.86	0.09	0.33	0.36
A754	0.52	5.68	1.01	4.66	6.59	A115	1.50	15.40	0.18	0.94	0.38
A3667	0.52	3.65	0.65	0.93	0.78	A2390	1.38	12.34	0.10	1.43	1.15
A2665	0.51	4.30	0.79	0.15	0.84	A2219	1.65	21.20	0.18	1.44	0.67
AS1101	0.53	1.45	0.24	1.50	2.73	ZWCL2341.1+0000	1.07	6.08	0.03	0.07	0.57
A2256	0.54	4.98	0.80	4.00	1.46	A2537	1.32	11.73	0.05	0.34	0.27
A1831	0.58	1.87	0.26	0.23	0.86	Bullet	1.58	20.15	0.09	0.98	0.35
A1795	0.58	4.07	0.55	0.80	0.16	A2744	1.30	11.36	0.05	0.82	0.91
A3112	0.68	3.42	0.32	7.54	7.97	MS1512.4+3647	0.76	2.46	0.01	0.20	0.93
A1800	0.69	2.41	0.22	0.22	0.37	RXCJ1347.5-1145	1.57	23.34	0.04	1.17	0.07

Note. Columns (1) and (6) show the spectral extraction radius in Mpc, columns (2) and (7) are the estimated projected dark matter masses in the spectral extraction radii $M_{DM}^{proj}(R_{ext})$, the projected dark matter masses per luminosity distance M_{DM}^{proj}/D_L^2 are given in columns (3) and (8), columns (4), (5), (9), and (10) show the weighting factors (ω_{cnt}) calculated based on the total counts in the fitting band 2–6 keV and the weighting factors (ω_{dm}) calculated based on the predicted dark matter flux. These factors are used to stack the ARFs and RMFs of each cluster in the sample.
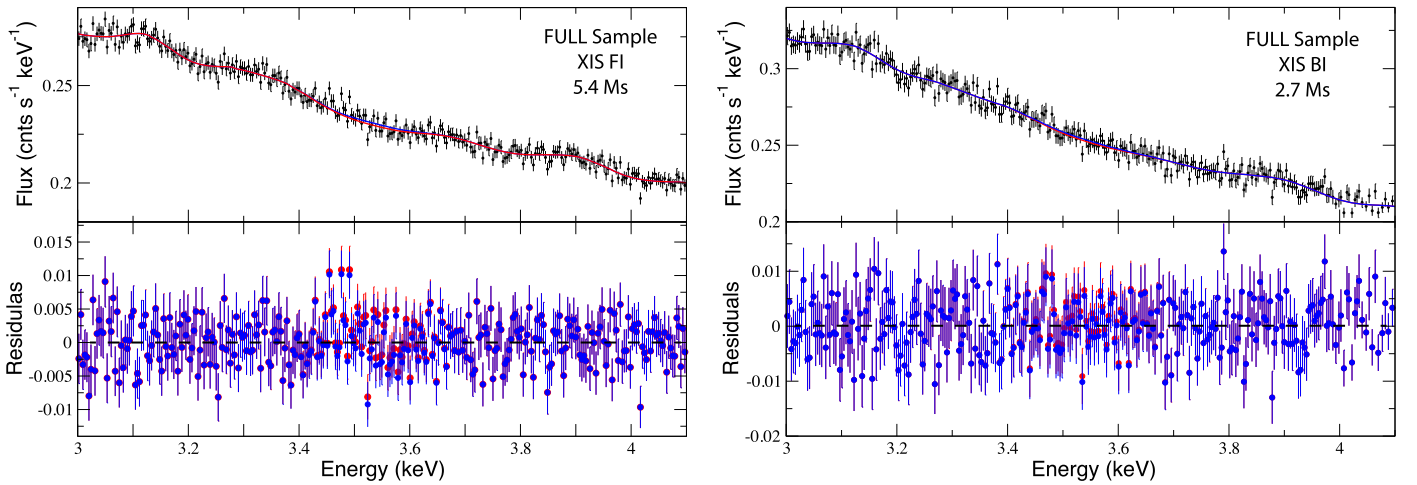

Figure 1. The 3–4 keV band of the binned stacked *Suzaku* XIS FI (left panel) and XIS BI (right panel) spectra of the full sample. The figures show the energy band where the unidentified 3.5 keV line is detected by Bu14a. Gaussian lines with maximum values of the flux normalizations of K XVIII and Ar XVII DR are already included in the models. The 3.5 keV line is not significantly detected in either of these samples. The red and blue model lines in the top panels show the total model before and after a Gaussian line is added at 3.54 keV. Bottom panels show the residuals before (red) and after (blue) the Gaussian line is added.

cluster is given in Table 3 for each cluster in the full *Suzaku* sample.

Initially, we examine the 3–4 keV band of the stacked FI observations of the full sample. After the addition of the Gaussian model at 3.54 keV, the new best-fit χ^2 becomes 1028.1 for 1068 dof. The change in the χ^2 is 4.1 after the addition of a dof. The best-fit flux of the line is $1.0^{+0.5}_{-0.5}$ ($^{+1.3}_{-0.9}$) $\times 10^{-6}$ phts cm^{-2} s^{-1}.

The change in the χ^2 corresponds to a 2σ detection for an additional degree of freedom in the stacked FI observations of the full sample. The stacked XIS FI spectrum of the full sample, and the best-fit models before and after the Gaussian line is added, are shown in Figure 1 left panel.

For the BI observations of the full sample, the fit with *line-free apec* model and additional Gaussians for known
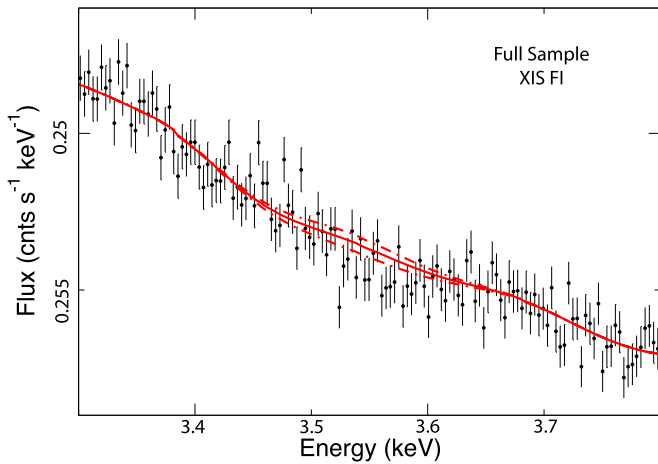
Figure 2. Zoomed-in *Suzaku* XIS FI spectrum of the stacked full sample. The solid red line shows the best-fit line flux scaled from the *XMM-Newton* MOS full sample detection (4×10^{-6} phot s^{-1} cm^{-2}), under the dark matter decay scenario. The dashed lines mark the 90% confidence levels of the scaled flux.

atomic lines give a good-fit with χ^2 of 1111.5 (1078 dof). The line is not detected at a statistically significant level in this spectrum. An additional Gaussian line at 3.54 keV improves the fit by $\Delta\chi^2 = 1.5$ for an extra dof (the χ^2 becomes 1109.9 for 1077 dof). The best-fit flux of the line is $9.1^{+1.5}_{-7.3}$ $(^{+2.2}_{-9.1}) \times 10^{-7}$ phts cm^{-2} s^{-1}. The stacked XIS BI spectrum of the full sample and the best-fit models before and after the Gaussian line is added at 3.54 keV are shown in Figure 1, right panel.

To test the decaying dark matter origin of the signal, we further investigate if the mixing angles indicated by these fluxes are consistent with the previous detections in the literature. The measured flux from a mass of dark matter within the FOV can be converted into the decay rate, assuming dark matter particles decaying monochromatically with $E_\gamma = m_s/2$. The mixing angle for this decay is

$$\sin^2(2\theta) = \frac{F_{\mathrm{DM}}}{12.76 \ \mathrm{cm}^{-2} \ \mathrm{s}^{-1}} \left(\frac{10^{14} \ M_\odot}{M_{\mathrm{DM}}^{\mathrm{FOV}}} \right)$$
$$\left(\frac{D_L}{100 \ \mathrm{Mpc}} \right)^2 \left(\frac{1}{1+z} \right) \left(\frac{1 \ \mathrm{keV}}{m_s} \right)^4, \qquad (2)$$

where F_{DM} is the observed flux due to dark matter decay (Pal & Wolfenstein 1982) and is related to the surface density or flux of decaying dark matter particles within the FOV;

$$F_{\mathrm{DM}} = \frac{M_{\mathrm{DM}}^{\mathrm{FOV}}}{4\pi D_L^2} \frac{\Gamma_\gamma}{m_s} (1+z) \ \mathrm{photons} \ \mathrm{cm}^{-2} \ \mathrm{s}^{-1}, \qquad (3)$$

where Γ_γ and m_s are the decay rate and dark matter particle mass, respectively.

Using ω_{dm} and the projected dark matter masses given in Table 3, we find that the weighted projected dark matter mass-per-distance squared of the full *Suzaku* sample is 1.17×10^{10} $M_\odot$ Mpc^{-2}. Using Equation (2), one can calculate the mixing angle to be $\sin^2(2\theta) = 2.7^{+1.4}_{-1.4}$ $(^{+3.4}_{-2.3}) \times 10^{-11}$ for the full *Suzaku* FI sample, for a particle mass of $m_s = 7.08$ keV. The associated 90% upper limit to the mixing angle is $\sin^2(2\theta) < 6.1 \times 10^{-11}$ in this sample. To compare the consistency between XIS FI spectrum and the previously detected line flux in *XMM-Newton* observations (Bu14a), we

scale the flux based on the signal from the larger cluster sample, under the dark matter decay scenario. Figure 2 shows the zoomed-in 3.3–3.8 keV band of the stacked XIS full FI sample spectrum. The solid line marks the best-fit flux of the 3.54 keV line, scaled from the Bu14a full sample flux, with the 90% uncertainties marked by dashed lines. As the figure clearly shows, the XIS FI observations are consistent with the *XMM-Newton* observations at a 90% level.

The *Suzaku* BI observations of the full sample give a mixing angle measurement of $\sin^2(2\theta) = 2.5^{+0.4}_{-1.9}$ $(^{+5.9}_{-2.4}) \times 10^{-11}$ for the same weighted mass-per-distance squared. These are given in Table 4. The *Suzaku* full FI/BI sample measurements are consistent with each other. The mixing angles measured from the full *XMM-Newton* MOS/PN samples ($\sin^2(2\theta) = 6.8^{+1.4}_{-1.4}$ $(^{+2.0}_{-3.0}) \times 10^{-11}$) are consistent at a 1σ confidence level, and the MOS observations of bright clusters (Coma+Ophiuchus+Centaurus; $\sin^2(2\theta) = 1.8^{+0.44}_{-0.39}$ $(^{+1.2}_{-1.2}) \times 10^{-10}$) are consistent at a $\sim2.7\sigma$ confidence level (see Bu14a). The core excised observations of the Perseus cluster ($2.3^{+0.7}_{-0.7}$ $(^{+1.2}_{-1.2}) \times 10^{-10}$; see Bu14a) measurement are in tension with the present *Suzaku* sample result at a level of $\sim2.5\sigma$. Comparison of mixing angles measured from *Suzaku* samples with the previous detections and limits are shown in Figure 3.

3.2. Cool-core Clusters

We now divide the full sample into two independent subsamples, in order to investigate whether the line flux correlates with the presence of cool gas in the intra-cluster plasma. The clusters are divided into cool-core clusters (CC) and non-cool-core clusters (NCC), based on previous identifications in the literature. If, indeed, the flux of the 3.5 keV line is stronger in the stacked cool-core cluster sample (i.e., if a correlation is observed between gas temperature and the flux), this would be a strong indication that the 3.5 keV line is astrophysical in origin. The classification of each cluster is given in Table 1. For some of the clusters in the full sample (e.g., A2495, A2249, A272, RXC J2218.8-0258, MS 2216.0-0401, and A566) the X-ray studies with high angular resolution observatories, e.g., *Chandra* and *XMM-Newton*, are not available in the literature. Due to the relatively large point-spread-function ($\sim2'$ half-power diameter) of the *Suzaku* mirrors, we cannot distinguish if these clusters have cool intra-cluster gas in their center. Hence, we exclude these clusters from both subsamples.

We have performed the stacking process following the same approach outlined in Section 2 for the CC clusters. A total of 3.1 Ms of good stacked FI and 1.5 Ms BI observations are obtained in this subsample. The weighted mean redshift of the subsample is 0.13. The stacked FI/BI observations of this subsample contain 52% and 51% of the total source counts of the full FI and BI observations.

We fit the stacked *Suzaku* FI spectra of the CC cluster as described in Section 3. The best-fit temperatures, normalizations, and fluxes of S XV, S XVI, Ca XIX, and Ca XX are given in Table 2. Cl Lyα at 2.96 keV is not detected significantly in this spectrum; therefore, we exclude the Cl Lyβ line at 3.51 keV from our fits. Overall, we obtain a good fit to the stacked CC spectrum with $\chi^2 = 1130.0$ (1068 dof). Adding an extra Gaussian model to the MOS spectrum at 3.54 keV does not improve the fit significantly ($\Delta\chi^2 = 1.68$) for an additional dof, and results in a non-detection. The 90% upper limit on the flux of this line at 3.54 keV is 1.4×10^{-6}

Table 4
Measured Flux of the 3.5 keV Line in the Stacked *Suzaku* Clusters

Sample	(1) Inst.	(2) Energy (keV)	(3) Flux $(10^{-6}$ phts cm^{-2} s$^{-1})$	(4) χ^2 (dof)	(5) $\Delta\chi^2$ (dof)	(6) $M_{\rm DM}^{\rm proj}/D_L^2$ $(10^{10}\ M_\odot\ {\rm Mpc}^{-2})$	(7) $\sin^2(2\theta)$ (10^{-11})
Full Sample	FI	3.54	$1.0^{+0.5}_{-0.5}\ (^{+1.3}_{-0.9})$	1028.1 (1068)	4.11 (1)	1.17	$2.7^{+1.4}_{-1.4}\ (^{+3.4}_{-2.3})$
	BI	3.54	$0.9^{+0.2}_{-0.7}\ (^{+0.2}_{-0.9})$	1109.9 (1077)	1.46 (1)	1.17	$2.5^{+0.4}_{-1.9}\ (^{+5.9}_{-2.5})$
Cool-core	FI	3.54	<1.4	1131.7 (1069)	1.68 (1)	1.06	<5.1
Clusters	BI	3.54	<2.1	1143.0 (1072)	0.15 (1)	1.06	<6.1
Non-cool Core	FI	3.54	$2.0^{+1.0}_{-0.7}\ (^{+1.9}_{-1.2})$	1034.7 (1075)	6.56 (1)	1.19	$5.3^{+2.6}_{-1.8}\ (^{+4.7}_{-3.1})$
Clusters	BI	3.54	<5.4	1159.9 (1072)	0.51 (1)	1.19	<14.1

Note. Columns (2) and (3) are the rest energy and flux of the unidentified line in the units of photons cm^{-2} s^{-1} at the 68% (90%) confidence level. Columns (4) and (5) show the χ^2 after the line is added to the total model, and change in the χ^2 when an additional Gaussian component is added to the fit; column (6) is the weighted ratio of mass-to-distance squared of the samples; and column (7) shows the mixing angle limits measured in each sample. Reported constraining limits are at 90% confidence. Energies are held fixed during the model fitting.
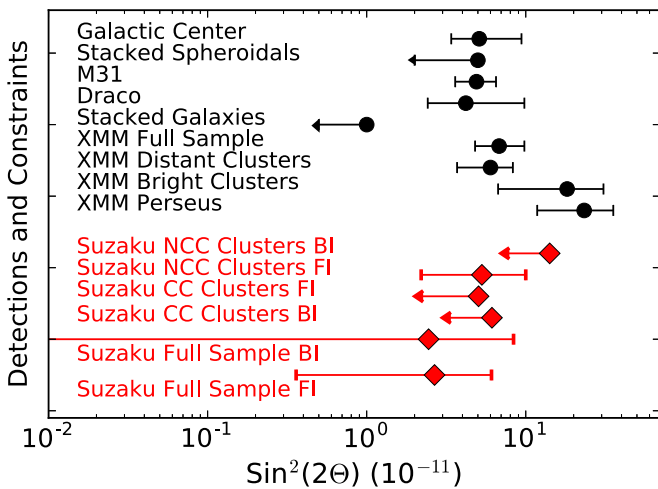

Figure 3. Comparison of sterile neutrino mixing angle upper limits, obtained from the stacked galaxy clusters observed with *Suzaku*. The results in the literature are also shown. The error bars and upper limits from this work and Bu14a results are at 90% confidence levels. The upper limits from the stacked spheroidal galaxies (Malyshev et al. 2014, 2σ) and stacked galaxies (Anderson et al. 2015, 90%), along with the detections in the Galactic center (Boyarsky et al. 2015, 90%), the Draco dwarf spheroidal (Ruchayskiy et al. 2015, 1σ), and M31 (Bo14a, 1σ) are shown. Anomalously high Perseus flux reported in Bu14a is clearly seen in the figure. We note that the particle mass is not compared here.

photons cm^{-2} s^{-1} from this spectrum. The upper limit on the flux can be translated to a mixing angle of 5.1×10^{-11} for a given projected dark matter mass-per-distance squared for the sample ($1.06 \times 10^{10}\ M_{\rm Sun}\ {\rm Mpc}^{-2}$). The mixing angle indicated by the stacked FI observations of CC clusters is consistent with the full *Suzaku* sample and the previous *XMM-Newton* detections.

We note that the discrepancy observed in plasma temperatures between FI and BI observations of the cool-core clusters might be due to the difference in the response of the FI and BI sensors, or the power-law normalizations for CXB that were left free during the fits. We note that spectra of individual clusters are rescaled to their emitter frame before being stacked. Therefore, the stacked spectra do not contain any physical meaning after the blue-shifting and stacking processes. The main goal of this work is to model the continuum accurately to make the analysis sensitive to faint line detections. Therefore, the observed difference is not worrying in the context of this

work. The crucial point is that the line ratios observed in FI and BI observations within each sample are consistent. The line ratios are used to determine the plasma temperature and fluxes' of faint lines in the 2.5–4.1 keV band.

The overall fit to the stacked BI observations to CC clusters is acceptable, with χ^2 of 1142.85 for 1068 dof. Adding an extra Gaussian line at 3.54 keV does not improve the fit significantly, and results in a non-detection. The 90% upper limit to the flux is 2.1×10^{-6} photons cm^{-2} s^{-1} from this spectrum; the upper limit on the mixing angle ($<6.1 \times 10^{-11} M_{\rm Sun}\ {\rm Mpc}^{-2}$) from this flux limit is consistent with the full-sample and FI detections.

3.3. Non-cool Core Clusters

We now examine the FI and BI observations of the NCC clusters. A total of 2.2 Ms good FI and 1.1 Ms good BI observations are obtained for this sample. The NCC cluster sample contains 46% of the total FI source counts, and 45% of the total BI source counts, for the full sample. The redshift has a weighted mean value at 0.11, and the projected dark matter mass-per-distance squared is $1.19 \times 10^{10}\ M_{\rm Sun}\ {\rm Mpc}^{-2}$ of the NCC subsample.

To be able to conservatively estimate the fluxes of the K XVIII, Cl XVII, and Ar XVII lines, we use the Ca XIX and Ca XX lines for this sample. Probing the 3–4 keV band, FI observations do not reveal significant residuals around 3.54 keV. Indeed, the first fitting attempt (without a Gaussian model at 3.54 keV) is an overall good fit with χ^2 of 1041.3 for 1076 dof. Addition of a Gaussian model improves the fit by $\Delta\chi^2$ of 6.56 for an extra dof. The best-fit flux of the line becomes $2.0^{+1.0}_{-0.7}\ (^{+1.9}_{-1.2}) \times 10^{-6}$ photons cm^{-2} s^{-1}. The mixing angle corresponding to this flux is $5.3^{+2.6}_{-1.8}\ (^{+4.7}_{-3.1}) \times 10^{-11}$, which is consistent with the full sample. The 90% upper limit of its flux is 3.9×10^{-6} phts cm^{-2} s^{-1} in the FI observations of the non-cool clusters, with a mixing angle of 1.0×10^{-10}.

Treating the stacked BI observations of the NCC clusters, we obtain an acceptable fit (χ^2 of 1159.4 with 1071 dof) without an additional Gaussian model at 3.54 keV. Adding an extra Gaussian component at 3.54 keV changes the goodness of the fit by $\Delta\chi^2$ of 0.51 ($\Delta{\rm dof} = 1$). The 90% upper limit of the flux of the line is 5.4×10^{-6} phts cm^{-2} s^{-1}, which corresponds to a mixing angle of 1.4×10^{-10} for this sample.

4. SUMMARY

Stacking X-ray spectra of galaxy clusters at different redshifts provides a sensitive tool to detect weak emission features. This method, tested on the *XMM-Newton* observations of 73 clusters (Bu14a), resulted in the detection of a very weak unidentified spectral line at ~3.5 keV. In this work, we take a similar approach and stack *Suzaku* FI (XIS0, XIS3) and BI (XIS1) observations of 47 nearby ($0.01 < z < 0.45$) galaxy clusters to look for the unidentified emission line. Our *Suzaku* sample consists of 5.4 Ms of FI and 2.1 Ms of BI observations. The total source counts collected in this study are less than those of the stacked *XMM-Newton* observations, by a factor of 1.8. The redshift span is slightly larger in the *Suzaku* full sample than the full *XMM-Newton* sample, leading to more effective smearing of the instrumental features. The redshift range of the full *Suzaku* sample corresponds to an energy difference of up to 1.44 keV at 3.5 keV, which is sufficient to smear out and eliminate the background or response features.

The stacked FI data for the full sample prefers an additional emission line at $E = 3.54$ keV (the energy fixed at the best-fit value for the *Suzaku* line detection in Perseus Franse et al. 2016), but only at 2σ confidence level, with a flux of $1.0^{+0.5}_{-0.5} \, (^{+1.3}_{-0.9}) \times 10^{-6}$ phts cm^{-2} s^{-1}. The statistics of the data set are insufficient to constrain the energy of this faint line. The line is not significantly detected in the BI observations; however, an additional Gaussian model improves the fit by $\Delta\chi^2 = 1.5$ and has a flux of $9.1^{+1.5}_{-7.3} \, (^{+2.2}_{-9.1}) \times 10^{-6}$ phts cm^{-2} s^{-1}. The fluxes observed in FI and BI observations are in agreement with each other.

In an attempt to investigate a possible correlation of the flux of the unidentified line with cooler gas in the ICM, we divide the full sample into two subsamples; CC and NCC clusters. If a correlation is observed, it would be an indication that the unidentified line is astrophysical in origin. Atomic lines are more prominent in cool-core clusters, where a significant amount of cooler gas with higher metal abundances resides in the core. However, we do not detect any significant spectral feature at 3.5 keV in the separate CC and NCC clusters. The FI observations of the NCC sample show a weak 2.4σ residual at 3.54 keV, with a flux of $5.3^{+2.6}_{-1.8} \, (^{+4.7}_{-3.1}) \times 10^{-6}$ phts cm^{-2} s^{-1}. The upper limits derived from these samples are consistent with previous detections. We note that both CC and NCC subsamples contain fewer source counts compared to all of the *XMM-Newton* samples studied in Bu14a, so the sensitivity of the presented *Suzaku* analysis is weaker. We also note that, due to smaller FOV and lower effective area of the *Suzaku* XIS detectors (compared to the *XMM-Newton* EPIC detectors), this analysis might be less sensitive to a weak signal from dark matter decay. The value of this analysis is in that it is independent and performed with a different instrument.

The upper limits provided by this work (full sample; $\sin^2(2\theta) = 6.1 \times 10^{-11}$) are in agreement with the detections in the combined M31, Galactic center observations ($\sin^2(2\theta) = 5$–7×10^{-11}; see Boyarsky et al. 2015), and results from deep MOS ($\sin^2(2\theta) < 5.8 \times 10^{-11}$) and PN ($\sin^2(2\theta) = 1.8$–$8 \times 10^{-11}$) observations of the Draco galaxy (Ruchayskiy et al. 2015). However, the line flux in the core of the Perseus cluster is in tension with the presented stacked *Suzaku* and *XMM-Newton* clusters and other detections (Bu14a, Franse et al. 2016). Studying the origin of the 3.5 keV line with CCD resolution observations of galaxy clusters and other astronomical objects appears to have reached its limit; the problem requires higher-resolution spectroscopy, such as that expected from *Hitomi* (Astro-H).

REFERENCES

Abazajian, K. N. 2014, PhRvL, 112, 161303
Anderson, M. E., Churazov, E., & Bregman, J. N. 2015, MNRAS, 452, 3905
Arnaud, K. A. 1996, in ASP Conf. Ser. 101, Astronomical Data Analysis Software and Systems V, ed. G. H. Jacoby & J. Barnes (San Francisco, CA: ASP), 17
Boyarsky, A., Franse, J., Iakubovskyi, D., & Ruchayskiy, O. 2015, PhRvL, 115, 161301
Boyarsky, A., Ruchayskiy, O., Iakubovskyi, D., & Franse, J. 2014, PhRvL, 113, 251301
Bulbul, E., Markevitch, M., Foster, A., et al. 2014a, ApJ, 789, 13
Bulbul, E., Markevitch, M., Foster, A. R., et al. 2014b, arXiv:1409.4143
Bulbul, E., Randall, S. W., Bayliss, M., et al. 2016, ApJ, 818, 131
Carlson, E., Jeltema, T., & Profumo, S. 2015, JCAP, 2, 009
Foster, A. R., Ji, L., Smith, R. K., & Brickhouse, N. S. 2012, ApJ, 756, 128
Franse, J., Bulbul, E., Foster, A., et al. 2016, arXiv:1604.01759
Gu, L., Kaastra, J., Raassen, A. J. J., et al. 2015, A&A, 584, L11
Horiuchi, S., Bozek, B., Abazajian, K. N., et al. 2016, MNRAS, 456, 4346
Iakubovskyi, D., Bulbul, E., Foster, A. R., Savchenko, D., & Sadova, V. 2015, arXiv:1508.05186
Jeltema, T., & Profumo, S. 2015, MNRAS, 450, 2143
Malyshev, D., Neronov, A., & Eckert, D. 2014, PhRvD, 90, 103506
Navarro, J. F., Frenk, C. S., & White, S. D. M. 1997, ApJ, 490, 493
Pal, P. B., & Wolfenstein, L. 1982, PhRvD, 25, 766
Protassov, R., van Dyk, D. A., Connors, A., Kashyap, V. L., & Siemiginowska, A. 2002, ApJ, 571, 545
Ruchayskiy, O., Boyarsky, A., Iakubovskyi, D., et al. 2016, MNRAS, 460, 1390
Smith, R. K., Brickhouse, N. S., Liedahl, D. A., & Raymond, J. C. 2001, ApJL, 556, L91
Tamura, T., Iizuka, R., Maeda, Y., Mitsuda, K., & Yamasaki, N. Y. 2015, PASJ, 67, 23
Urban, O., Werner, N., Allen, S. W., et al. 2015, MNRAS, 451, 2447
Vikhlinin, A., Burenin, R. A., Ebeling, H., et al. 2009, ApJ, 692, 1033